CONFERENCE PRE-PRINT

LINEAR AND QUASI-LINEAR PLASMA RESPONSE TO RESONANT MAGNETIC PERTURBATION DURING ELM MITIGATION IN HL-3

N. Zhang[1], Y. Q. Liu[2], G. Z. Hao[1], T. F. Sun[1] and G. Q. Dong[1]

[1]Southwestern Institute of Physics, P.O. Box 432 Chengdu 610041, China
[2]General Atomics, PO Box 85608, San Diego, CA 92186-5608, USA

Corresponding Author: zhangn@swip.ac.cn

Abstract:

Active mitigation of edge localized mode (ELM) with the odd parity of $n = 1$ (n is the toroidal mode number) resonant magnetic perturbation (RMP) has been recently achieved for the first time on the HL-3 tokamak. The linear and quasi-linear plasma responses to RMP fields are numerically investigated during ELM mitigation in HL-3, by utilizing the MARS-F and MARS-Q. The linear results show that RMP induces a strong edge peeling response, which is related to the ELM mitigation. The 50-degree phase shift for the $n = 1$ coil current between the upper and lower rows of the RMP coils presents the optimal coil phase. MARS-Q quasi-linear results show that: (i) without involving peeling-tearing instability near the plasma edge, the applied RMP has no side effects on the both toroidal momentum and radial particle transport in this HL-3 case; (ii) allowing weak peeling-tearing instability together with RMP produces finite flow damping and density pump-out level comparable to experiments; (iii) the modeled flow damping and density pump-out is not very sensitive to the assumed resistivity model (Spitzer vs uniform resistivity). It is also found that the neoclassical toroidal viscosity (NTV) due to 3D fields plays the key role in modifying the plasma momentum and particle transport in the HL-3.

1 Introduction

It is now well established that the resonant magnetic perturbation (RMP) technique is one of most effective method for type-I edge localized mode (ELM) control in high-confinement mode (H-mode) plasmas [1, 2, 3, 4, 5, 6]. Some key results have been obtained in recent years and reviewed in the Ref. [7]. Although the great successful for ELM control by RMP fields has been achieved, the physical mechanism of ELM control by RMP field has not been fully understood, yet. The RMP coil system is also designed for mainly ELM control in future magnetic confinement fusion devices, such as SPARC [8], ITER [9]. However, the toroidal asymmetry perturbation introduced by RMP can lead to some unwanted consequences and side effect on plasmas confinement, such as the density pump-out, toroidal flow braking, the modification of MHD instabilities. In general, these side effects are directly or indirectly related to the ELM suppression or mitigation. Understanding physics mechanisms of the particle and momentum transport due to RMPs is therefore essential for the better ELM control.

In recent, an array of 2×8 (poloidal$\times$toroidal) in-vessel RMP coil system the has been installed in HL-3 tokamak [12]. In addition, the mitigation of ELM has been successfully

achieved by the applying RMP fields after $t = 1800$ ms for the first time, as shown in figure 1. Moreover, figure 1(b) show that the line averaged electron density, measured by the CO_2 Laser interferometer, is slightly reduced by about 8% due to the RMP fields. The changes of the profiles of electron density and toroidal rotation velocity are further shown in figure 1(e). We observed that the edge electron density and toroidal rotation are slightly decreased by the RMP fields. In this work, we perform systematic linear and quasi-linear plasma response to resonant magnetic perturbation during ELM mitigation in HL-3 tokamak. We mention that the quasi-linear response focus on studying the self-consistently interplay between the $n \neq 0$ (n is toroidal mode number) RMP fields with the $n = 0$ plasma density and toroidal rotation frequency.

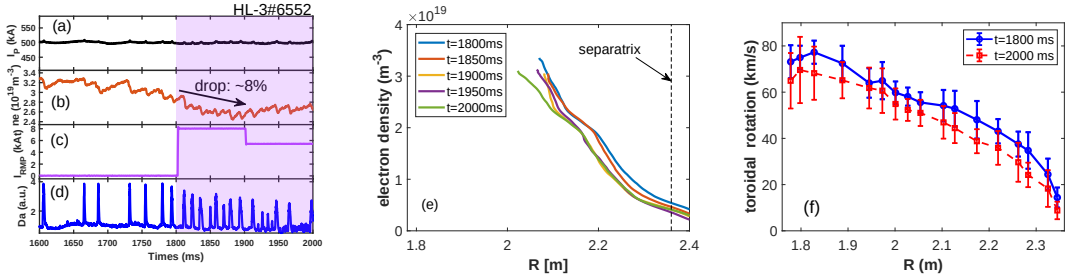

FIG. 1: Time traces of the HL-3 discharge 6552 showing (a) the plasma current, (b) the line averaged electron density, (c) the RMP coil current and (d) the D_α signal, with the shaded regions indicating the RMP duration time interval. (e) Radial profile of the electron density measured by the frequency modulated continuous wave reflectometry (FMCW) at t=1800, 1850, 1900, 1950 and 2000 ms, respectively. (f) Radial profiles of the plasma toroidal rotation velocity measured by the charge exchange recombination spectroscopy (CXRS) at t=1800 and t=2000 ms.

2 Computational model

In this work, the linear plasma response is described by the single fluid, resistive, full MHD equations in toroidal geometry [13]. The linearized equations can be written as

$$(\partial/\partial t + in\Omega)\rho = -\nabla \cdot [(\rho_{eq} + \Delta\rho_{n=0})\mathbf{v}] \tag{1}$$

$$(\rho_{eq} + \Delta\rho_{n=0})(\partial/\partial t + in\Omega)\mathbf{v} = -\nabla p + \mathbf{j} \times \mathbf{B} + \mathbf{J} \times \mathbf{b} - \rho R\Omega^2 \nabla R$$
$$-(\rho_{eq} + \Delta\rho_{n=0})[2\Omega\nabla\mathbf{Z} \times \mathbf{v} + (\mathbf{v} \cdot \nabla\mathbf{\Omega})R^2\nabla\phi] \tag{2}$$

$$(\partial/\partial t + in\Omega)\mathbf{b} = \nabla \times (\mathbf{v} \times \mathbf{B}) + (\mathbf{b} \cdot \nabla\Omega)R^2\nabla\phi - \nabla \times (\eta\mathbf{j}) \tag{3}$$

$$(\partial/\partial t + in\Omega)p = -\mathbf{v} \cdot \nabla P - \Gamma P \nabla \cdot \mathbf{v} \tag{4}$$

$$\mathbf{j} = \nabla \times \mathbf{b} \tag{5}$$

where (R, ϕ, Z) represents the cylindrical coordinates. The perturbed quantities ρ, $\mathbf{v}$, $\mathbf{b}$, $\mathbf{j}$ and p denote the perturbed plasma density, velocity, magnetic field, plasma current and pressure, respectively. The equilibrium quantities ρ_{eq}, $\mathbf{B}$, $\mathbf{J}$ and P are the plasma density, field, current and pressure. Ω is the toroidal rotation frequency. η is the plasma resistivity. $\Gamma = 5/3$ is the ratio of specific heats. $\Delta\rho_{n=0}$ represents the surface-averaged change to the equilibrium plasma density ρ_{eq}.

The external RMP field is produced by the source current density $\mathbf{j}_{RMP}$ that satisfies

$$\nabla \times \mathbf{b} = \mathbf{j}_{RMP}, \qquad \nabla \cdot \mathbf{j}_{RMP} = 0. \tag{6}$$

We mention that the source current is specified as a surface current at the location of RMP coils in MARS-F model. The current density $\mathbf{j}_{RMP}$ has an $\exp(in\phi)$ dependence along the toroidal angle ϕ. The above equations (1-6) are solved together with the vacuum equation outside the plasma and the thin resistive wall equations in the linear RMP response model.

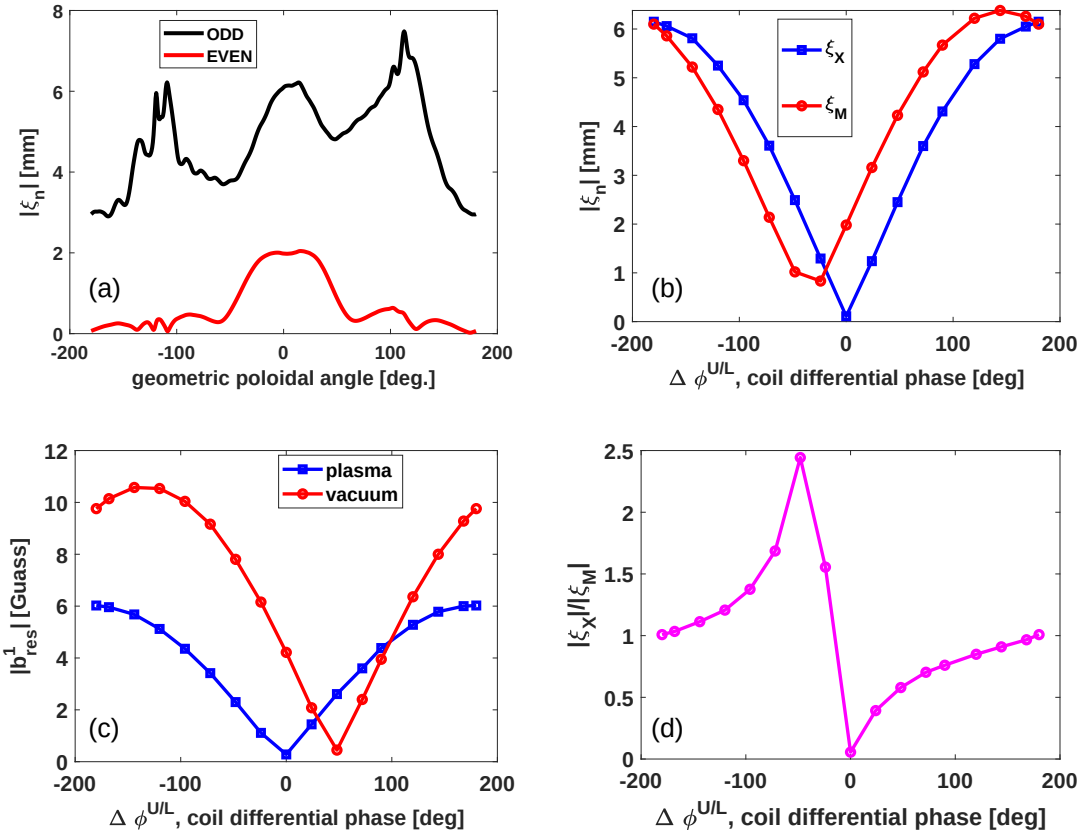

FIG. 2: Various computed response metrics while varying the coil phasing for the $n = 1$ RMP, showing (a) amplitude of the plasma surface displacement along the (geometric) poloidal angle between the odd (black) and even (red) parity configurations, (b) amplitude of the pitch resonant radial field component near the plasma edge, of the vacuum field (red) versus total field including the plasma response (blue), while scanning $\Delta\phi^{U/L}$, (c) amplitude of the plasma surface displacement at the low field side mid-plane (ξ_M, red) and near the X-point (ξ_X, blue) while scanning $\Delta\phi^{U/L}$, and (d) the ratio of the above two displacements (ξ_X/ξ_M). The RMP coil current is assumed to be 8 kAt.

The quasi-linear response MARS-Q model considered here are used to study the influence of the RMP on the toroidal momentum transport and radial particle transport [14]. The $n \neq 0$ resistive MHD response equations, together with the $n = 0$ toroidal momentum equilibrium equation and radial particle equilibrium equation are self-consistently solved as an initial value problem. More specifically, the following $n = 0$ toroidal momentum

balance equation can be written as

$$\frac{\partial L}{\partial t} = D(L) + T_{NTV} + T_{JXB} + T_{REY} + T_{source} \tag{7}$$

where $L \equiv \rho\langle R^2\rangle\Omega$ is the surface averaged toroidal momentum of the plasma, and $D(L)$ the momentum diffusion operator

$$D(L) = \frac{G}{s}\frac{\partial}{\partial s}\frac{s}{G}\left[\chi_M\langle|\nabla s|^2\rangle\frac{\partial L}{\partial s} + V_{pinch}\langle|\nabla s|\rangle L\right], \tag{8}$$

with $G \equiv F\langle 1/R^2\rangle$ being a geometric factor. F denotes the equilibrium poloidal current flux function. χ_M is the toroidal momentum diffusion coefficient. V_{pinch} is the velocity pinch term. T_{source} denotes the momentum source. More importantly, the three toroidal torques, acted as the momentum sink term, are considered here, including the the NTV torque (T_{NTV}), the resonant electromagnetic torque (T_{JXB}) and a torque associated with the Reynolds stress tensor (T_{REY}). Detailed expressions of these torques can be found in our previous work [15]. We also mention that the NTV torque here is computed by a semi-analytic model, where the various NTV regimes are smoothly connected [16].

We assume that a toroidal momentum balance has been established before the application of the RMP field, $D(L(t=0)) + T_{source} = 0$. In addition, we further assume that the RMP field does not modify the momentum source nor the momentum diffusion coefficient (χ_M). Therefore, the change of the toroidal momentum $\triangle L \equiv L(t) - L(0)$ relative to the initial value $L(0)$, can be written as

$$\frac{\partial(\triangle L)}{\partial t} = D(\triangle L) + T_{NTV} + T_{JXB} + T_{REY}, \tag{9}$$

Similarly, when assuming that the radial particle balance has been obtained before applying the RMP fields, the change of the plasma density, $\Delta\rho_{n=0}$, due to 3D perturbations is then obtained by solving

$$\frac{\partial\Delta\rho_{n=0}}{\partial t} = -\nabla\cdot(\rho\mathbf{v}) - \nabla\cdot(m\Gamma_{NTV}) + \nabla\cdot\chi_D\nabla(\Delta\rho_{n=0}), \tag{10}$$

where the first term of the right hand side of Eq. (10) ($\Delta n_{MHD} \equiv -\nabla\cdot(\rho\mathbf{v})$) is associated with the 'fluid' particle flux. The second term is related to the the neoclassical effect (due to 3D perturbations) which is beyond the standard single-fluid MHD model. The last term denotes the effect of particle radial diffusion.

For the change of the $n = 0$ toroidal momentum (9) and plasma density (10), we assume a free boundary condition at the plasma center, while Dirichlet fixed boundary condition is considered at the plasma edge in this work. A semi-implicit, adaptive time advance scheme is devised for solving the above quasi-linear equations. The MARS-Q formulation has been well validated against in several device experiments [17, 18, 19, 20].

3 Modeling results

Figure 2(a) compares the MARS-F computed amplitude of the surface displacement along the poloidal angle, for the odd and even coil parities respectively. It can be observed that the odd parity coil configuration triggers the larger displacement amplitude than

that of the even parity coils. In addition, the displacement caused by even parity coils predominantly peaks near the outboard mid-plane of torus, indicating the type of core kink response. We point out that this core kink response need to be avoided for the following reasons: (i) it has limited effect on the pedestal transport, thus does not facilitate the ELM control; (ii) the core kink response could damp the core plasma rotation and further deteriorates the level of core plasma confinement [19]; (iii) the core kink response may lead to mode locking [21, 22]. In order to predicted the optimal phasing of $n = 1$ RMP

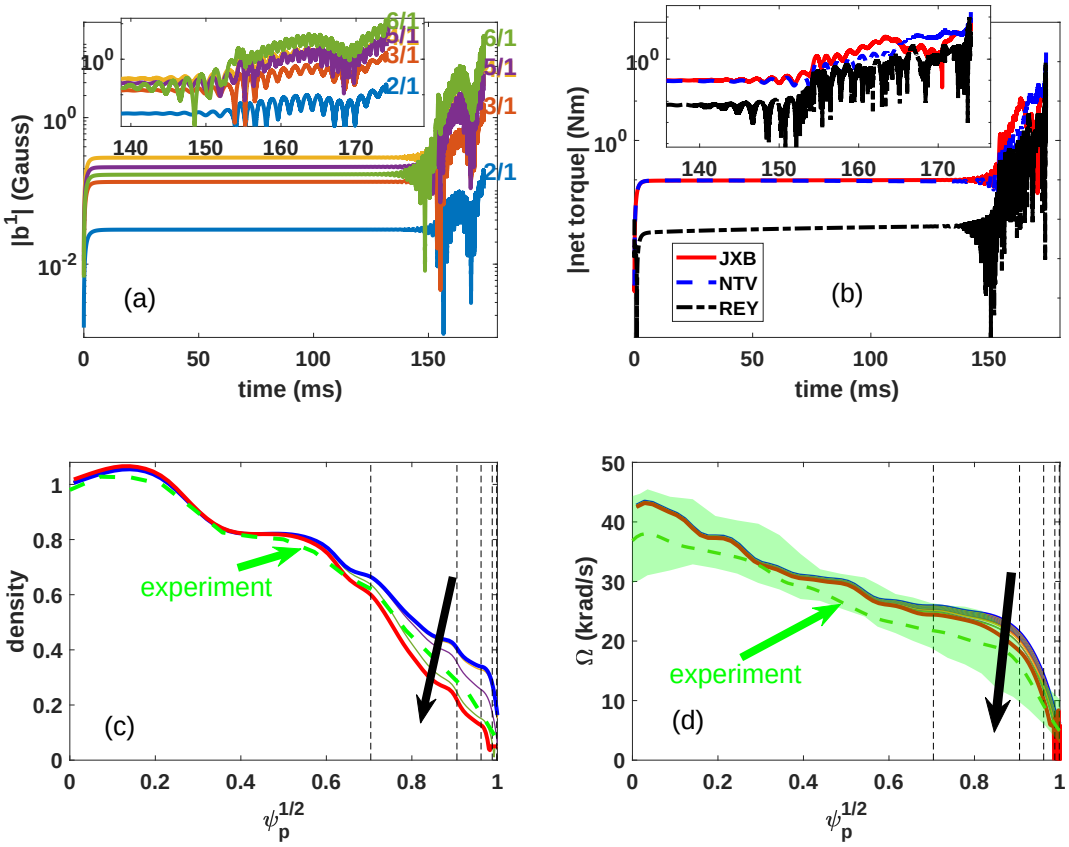

FIG. 3: The MARS-Q quasi-linear initial-value simulation results for the HL-3 discharge 6552, showing time traces of various (a) resonant radial field components ($m/n = 2/1, \cdots, 6/1$) at the corresponding rational surfaces and (b) net toroidal torques, and radial profile evolution of (c) the (normalized) plasma density and (d) the plasma toroidal rotation frequency. Shown in (c-d) are 41 time slices selected at equal period, with the thick blue curve indicating the initial profile prior to the RMP application, the thick red curve indicating the profile at the end of simulation, and black arrows indicating the time flow. For comparison, dashed green curves in (c-d) show the experimentally measured profiles at 2000 ms. The shaded region in (d) also indicates the measurement uncertainty. Assumed is 8 kAt current for the RMP coils in odd parity and in the $n = 1$ configuration, as well as the Spitzer model for the plasma resistivity.

coil configuration in HL-3, we further report the MARS-F computed plasma response to RMP with full scanning toroidal phasing of coil currents ($\Delta\phi^{U/L}$) from -180 degree to +180 degree. Figure 2(a) shows the amplitudes of normal displacement (ξ_n) near the X-point (denoted by ξ_X) and the outboard mid-plane (denoted by ξ_M), versus coil phasing $\Delta\phi^{U/L}$. Figure 2(c) shows that the dependence of the amplitude of the outmost pitch resonant radial field component ($|b^1_{res}|$) on the coil phasing $\Delta\phi^{U/L}$. Here the 'vacuum' and

'plasma' represent the vacuum field and total field including plasma response, respectively. This quantity $|b^1_{res}|$ characterizes the plasma edge screening due to the resistive plasma response. The magnitude of $|b^1_{res}|$ also determines the size of the magnetic island near the plasma edge. There are several observations from these plots. First of all, we find that the plasma response to RMP field is very sensitive to coil phasing $\Delta\phi^{U/L}$. Secondly, as shown in figure 2(b), the larger phase difference ($\Delta\phi^{U/L}$) between the upper row and the lower row coils ($n = 1$) can generally cause the larger plasma displacement near both the X-point and mid-plane region of torus in this HL-3 plasmas. Figure 2(c) shows that the resistive plasma response model obviously modifies the dependence relationship of pitch resonant radial field component $|b^1_{res}|$ on coil phasing. We also find that, compared with vacuum field, the response field amplitude can be amplified or even reduced, depending on the coil phasing. There is an about 50 degree phase shift between the vacuum and resistive plasma model computed fields. Thirdly, there is the similar trend for the quantities ξ_X and $|b^1_{res}|$ of response fields versus the coil phasing $\Delta\phi^{U/L}$, indicating that the edge peeling response (X-point displacement) is well correlates with edge island size. We also mention that this edge peeling criterion works not only for ELM mitigation but also for ELM suppression [23].

We point out that the strategy for choosing RMP configuration for best ELM control is that maximizing edge peeling response, and meanwhile minimizing core kink response. Figure 2(d) shows the the ratio ξ_X/ξ_M of the X-point displacement to the outboard mid-plane displacement. We find that the 50 degree phase shift is the best choice for ELM control. This computed optimal coil phasing is still verified in the future HL-3 experiments.

In the following, we shall report the toroidal momentum transport (rotation damping) and radial particle transport (density pump-out) results from the MARS-Q initial-value quasi-linear simulations. The computed results are summarized in figure 3. Here the coil phasing is also setting as experiment (odd parity). In this simulation, both the particle radial diffusion coefficient (χ_D) and the toroidal momentum diffusion coefficient (χ_M) are assumed to be about 0.1 m^2/s at the magnetic axis, with a radial profile that scales as $T_e^{-3/2}$ (to be referred to as the Spitzer-like model hereafter). Plots (a) and (b) show the time traces of the amplitudes of the resonant field component and the net three toroidal torques (integrated over the plasma volume), respectively. The time evolutions of the radial profile of plasma density and toroidal rotation are plotted in figure 3(c) and 3(d). It should be point out that the whole process evolves in a self-consistently manner within the MARS-Q model.

As shown in figure 3(a), the RMP penetration process mainly involves two stages in this MARS-Q simulation. The first stage is from the start time of simulation to about t =140 ms, while the second stage is after the simulation time of 140 ms. We can observe that the penetrated resonant field components saturate at a very small amplitude during this first stage, indicating that a marginal stable edge peeling response field is triggered. Figure 3(b) shows that the computed net toroidal torques are relatively weak, and thus producing the no side effect on the density pump-out and rotation damping. It is also noted that the radial components of the resonant magnetic field are gradually increased after the simulation time of $t > 140$ ms. The $m/n = 6/1$ component of resonant field is dominant over the other components. It means that the edge peeling-tearing instability is evolving at this second stage. Furthermore, we find that the edge peeling-tearing mode grows non-monotonically, as the result of the time evolution of plasma rotation during the RMP penetration. It is more interesting that this weak peeling-tearing instability together

with RMP produces the finite rotation damping and density pump-out level comparable to experiments, as shown in figure 3(c) and 3(d).

In order to determine the physical mechanism of toroidal momentum and radial particle transports, we further show the radial profile of the toroidal torque density and the particle flux due to the particle diffusion, NTV flux and MHD terms, respectively, at the simulation time of $t = 170$ ms. We observed that the toroidal torques are localized in the edge, as shown in figure 4(a). In addition, both the JXB and NTV torques are comparable to each other, indicating that these two torques play the dominant role on the rotation damping. On the other hand, as shown in figure 4(b), a positive peak value of the NTV flux means outward particle transport, while a negative peak value of the particle flux due to MHD term provides inward transport. As expected, the particle diffusion term can also lead to the particle outward transport. It is should be pointed out that the MARS-Q

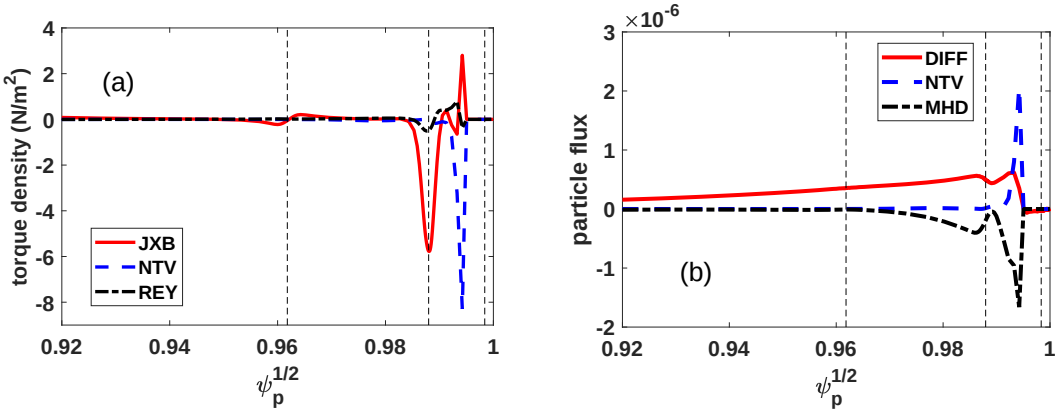

FIG. 4: Radial profiles of various (a) toroidal torque, and (b) radial particle flux, sink/source terms due to the applied $n = 1$ RMP field and obtained towards the end of the MARS-Q simulation ($t = 170$ ms) as reported in Fig. 3. Compared are the electromagnetic ('JXB' in red), NTV (in blue) and Reynolds stress ('REY' in black) torque densities in (a), and particle fluxes due to radial diffusion (red), NTV (blue) and MHD terms associated with the velocity perturbation (black) in (b). Vertical dashed lines indicate radial locations of the $q = 4, 5, 6$ surfaces, respectively.

simulation is terminated after the edge magnetic islands become enough large, due to the fact that the quasi-linear model cannot properly capture fully non-linear process any more.

4 Summary and conclusion

The active control of ELM has been successfully achieved by the $n = 1$ external 3D fields in HL-3 tokamak, produced by the new installed RMP coils. The MARS-F and MARS-Q codes are applied to computationally modelled the linear and quasi-linear response to RMP fields respectively, for this HL-3 ELM control experiments. We systematically investigate the effect of toroidal phasing between the upper and the lower coils current on the response fields. The RMP fields induced toroidal momentum transport and radial particle momentum are further modeled by the quasi-linear initial value MARS-Q code. The MARS-Q computations can be compared with the experimental observations. Finally, it is worthwhile to point out that these computed linear and quasi-linear results should be a useful consideration when designing the future RMP experiments in HL-3 tokamak.

Acknowledgments

This work is supported by National Magnetic Confinement Fusion Energy R&D Program under Contact Nos. 2022YFE03060002, 2022YFE03040001, the China National Nuclear Corporation Fundamental Research Program (No. CNNC-JCYJ-202236). This work is also partly supported by US DoE Office of Science under Contract DE-FG02-95ER54309 and DE-FC02-04ER54698.

References

[1] Evans T.E. *et al. Phys. Rev. Lett.* **92**, 235003 (2004).

[2] Liang Y. *et al. Phys. Rev. Lett.* **98**, 265004 (2007).

[3] Kirk A. *et al. Plasma Phys. Control. Fusion* **53**, 065011 (2011).

[4] Suttrop W. *et al. Phys. Rev. Lett.* **106**, 225004 (2011).

[5] Jeon Y.M. *et al. Phys. Rev. Lett.* **109**, 035004 (2012).

[6] Sun Y. *et al. Phys. Rev. Lett.* **117**, 115001 (2016).

[7] Fenstermacher M.E. *et al. Nucl. Fusion* **65**, 053001 (2025).

[8] Hughes J.W. *et al. J. Plasma Phys.* **86** 865860504 (2020).

[9] Lang P.T *et al. Nucl. Fusion* **53**, 043004 (2013).

[10] Schaffer M.J. *et al. Nucl. Fusion* **48**, 024004 (2008).

[11] Loarte A. *et al. Nucl. Fusion* **54** 033007 (2008).

[12] Wang A. *et al. Fusion Eng. Des.* **208** 114702 (2024).

[13] Liu Y.Q. *et al. Phys. Plasmas* **7** 3681 (2000).

[14] Liu Y.Q. *et al. Phys. Plasmas* **20** 042503 (2013).

[15] Zhang N. *et al. Phys. Plasmas* **24** 082507 (2017).

[16] Shaing K.C. *et al. Nucl. Fusion* **50** 025022 (2010).

[17] Liu Y.Q. *et al. Nucl. Fusion* **51** 083002 (2011).

[18] Liu Y.Q. *et al. Plasma Phys. Control. Fusion* **54** 124013 (2012).

[19] Zhang N. *et al. Nucl. Fusion* **60** 096006 (2020).

[20] Zhang N. *et al. Nucl. Fusion* **63** 086019 (2023).

[21] Yu Q.Q. *et al. Nucl. Fusion* **48** 024007 (2008).

[22] Shiraki D. *et al. Plasma Phys. Control. Fusion* **57** 025016 (2015).

[23] Zhou L.N. *et al. Nucl. Fusion* **58** 076025 (2018).